SCHOOL OF COMPUTATION, INFORMATION AND TECHNOLOGY — INFORMATICS

TECHNISCHE UNIVERSITÄT MÜNCHEN

Bachelor's Thesis in Informatics

Comparing Different Decomposition Methods to Approximate the Exponential Sum Bath Correlation Function

Benedict Blaschko

SCHOOL OF COMPUTATION, INFORMATION AND TECHNOLOGY — INFORMATICS

TECHNISCHE UNIVERSITÄT MÜNCHEN

Bachelor's Thesis in Informatics

Comparing Different Decomposition Methods to Approximate the Exponential Sum Bath Correlation Function

Vergleich verschiedener Zerlegungsmethoden zur Annäherung an die Exponentialsummen-Bad-Korrelationsfunktion

Author:	Benedict Blaschko
Examiner:	Prof. Dr. Christian B. Mendl
Supervisor:	Richard Milbradt
Submission Date:	27.09.2024

I confirm that this bachelor's thesis is my own work and I have documented all sources and material used.

Munich, 27.09.2024 Benedict Blaschko

Acknowledgments

Special thanks to our supervisor, Richard Milbradt, for his guidance and support throughout the thesis. His expertise and constructive feedback have been valuable in shaping this work, and we appreciate his dedication throughout the process.

We want to acknowledge the assistance digital tools provided throughout the writing process. We utilized OpenAI's ChatGPT, specifically versions GPT-3 and GPT-4, to explore concepts and refine the clarity of our arguments. Additionally, Grammarly was employed to enhance the grammar, style, and readability of the final manuscript. These tools served as supplementary aids, and we thoroughly reviewed and revised all content to ensure its accuracy and originality.

Abstract

We study decompositions of the bath correlation function using a Debye and Ohmic spectral density. These decompositions are based on the Residual theorem to produce a sum of exponentials. We used the Laurent series expansion to simplify the Bose function. The residue theorem and Laurent expansion yield results for the Debye spectral density, though they do not provide sufficient accuracy for the Ohmic spectral density.

Contents

Acknowledgments **iv**

Abstract **v**

1. Introduction **1**

2. Background **2**
2.1. Open quantum systems 2
2.2. Spectral density 4
2.3. Bose function 5
2.4. Laurent expansion 6
2.5. Continuum of bath modes 7
2.6. Residue theorem 8

3. Related Work **11**
3.1. Exponential sum decomposition 11
3.2. Methods based on the exponential sum decomposition 11
3.3. Bath correlation function 12
3.4. Spin-boson model 12
3.5. This work's objective 12

4. Results **13**
4.1. Numerical validation framework 13
4.2. Utilizing the residue theorem 15
4.3. Laurent expansion 18
4.4. Ohmic spectral density 19
4.5. Comparing different temperature regimes 20
4.5.1. Debye spectral density 20
4.5.2. Ohmic spectral density 21

5. Discussion **23**
5.1. Numerical reference framework 23
5.2. Residue theorem 23

5.3. Parameters of spectral densities 24
5.4. Laurent expansion 24

6. Conclusion **25**

A. Residue theorem **26**
A.1. Derivation for the Debye spectral density 26
A.1.1. Residuum at $i\gamma$ 26
A.1.2. Residuum at $z_k = 2\pi ik$ 27
A.2. Derivation for the Debye spectral density with Laurent expansion . . . 29
A.2.1. Residuum at $i\gamma$ 30
A.3. Derivation for the Ohmic spectral density 31
A.3.1. Residuum at $z_k = 2\pi ik$ 31

List of Figures **33**

Bibliography **35**

1. Introduction

An open quantum system develops memory effects while coupled to a target, such as a qubit, atom, or molecule. These memory effects vary over time and can be expressed by the bath correlation function [SCE15]. We decompose this function into a sum of exponentials. This representation holds significant benefits with subsequent calculations, e.g., the hierarchy of pure states to solve open quantum system dynamics with non-Markovian structured environments [SES14].

Quantum systems are volatile due to influences from their environment, which is called bath. The bath is modeled as a series of vibrating particles called the spin-boson model. These particles develop strong connections and influence each other, known as coupling. On the other hand, a relaxation behavior causes the return of these particles to a state of balance with their environment after being disrupted [Bre+84].

The spin-boson model has obtained a rising interest in the field of quantum computing. Researchers are interested in modeling long coherence times and being able to engineer parts of the properties of a quantum system, e.g., superconducting qubits coupled to their control and readout electronics [WKV04]. Aspects of quantum systems are of growing importance for biological simulations. The spin-boson model allows to describe extremely low temperatures and account for a vast number of vibrators. Key aspects of the simulation are coupling behaviors between proteins or energy transfers. [XS94]

In summary, many microscopic phenomena in science are modeled as an open quantum system, which can be further described using the bath correlation function [GM06][SS11]. This function includes integrals that cannot easily be solved analytically. We compare decomposition methods to find solutions for the exponential sum bath correlation function. We approximate parts inside the function and tested them numerically. The code that was used to generate all plots in this thesis is openly available under [Bla24].

2. Background

2.1. Open quantum systems

Numerous phenomena in science are modeled by open quantum systems which predict their behaviors. These systems contain nontrivial internal dynamics, as they do not behave according to classical mechanics. They experience loss of energy to the environment (dissipation), entanglement between the system and its environment, or the loss of a superposition (decoherence) [GPW99]. These effects are well described by the spin-boson model [GM06] [GOA94] [Leg+87] [GPW99]. This model revolves around particles called Bosons, which are subatomic particles with an integer spin. A Boson oscillates at a frequency and appears in a distinct energy level, which enables an exchange of energy when coupled to another particle. We can quantify the Boson's correlation effect on a distinct target over time using the bath correlation function [SCE15].

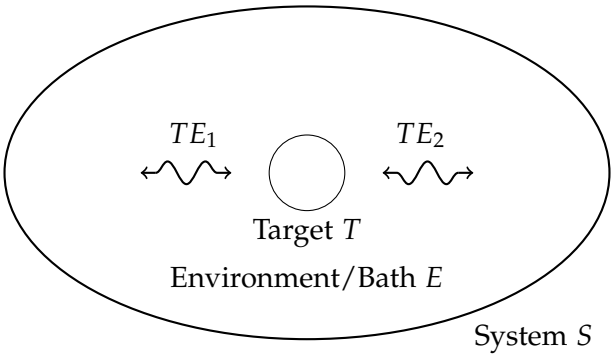

Figure 2.1.: Schematics of the system S consisting of the target T, the environment E, and interactions TE_k

An open quantum system S includes a target T, e.g., a molecule, an atom, or a quantum bit (qubit), and an environment E. The system's energy (Equation 2.1) is described by the Hamiltonian H_S.

$$H_S = H_T + H_E + H_{TE} \tag{2.1}$$

The environment/bath E is a sum of K linearly coupled harmonic oscillators connected to the target T. A harmonic oscillator is a common tool to model an environment by reducing it to particles [GOA94]. In our model, these particles are represented by frequency ω_k.

$$H_E = \sum_{k=1}^{K} \hat{\omega}_k \hat{a}_k^\dagger \hat{a}_k \tag{2.2}$$

The Hamiltonian of the environment is expressed as a sum of the Boson's frequency multiplied by bosonic creation and annihilation operators, $\hat{a}_k^\dagger$ and $\hat{a}_k$, as shown in Equation 2.2 [Sap23] [SCE15].

The harmonic oscillators are represented as frequency-specific bath modes. Figure 2.2 is a simplified illustration of the two bath modes, visualized as harmonic oscillators with three states. They are manipulated by the bosonic creation and annihilation operators, $\hat{a}_k^\dagger$ and $\hat{a}_k$. The resulting Bosons interact with the target T, with a coupling strength of $L_k\gamma_k$.

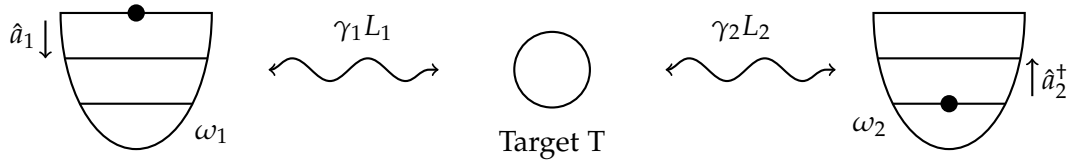

Figure 2.2.: Two bath modes as harmonic oscillators with three states at frequency ω_k, each linearly interacting with target T, with coupling strength $L_k\gamma_k$

The Hamiltonian for the interaction between target and environment H_{TE} is expressed in Equation 2.3 as the sum of the respective coupling strength $L_k\gamma_k$ of each bath mode multiplied by the kth bosonic creation operator $a_k^\dagger$, and the transposed complex conjugate $h.c.$

$$H_{TE} = \sum_{k=1}^{K} \left(\gamma_k L_k \cdot \hat{a}_k^\dagger + h.c. \right) \tag{2.3}$$

We visualized these bath modes with an illustrated thought experiment in Figure 2.3, which consists of two pendulums, each connected by a spring to target T in the center, and swinging from a pole at the respective edges of the system at different frequencies ω_1 and ω_2. The springs, connecting the pendulums to the target, represent the coupling strength $L_k\gamma_k$ of the bath modes.

The energy level of a bath mode is observed to be correlated with its frequency. The spectral density function $S(\omega)$ maps each frequency to their corresponding energy density [SCE15].

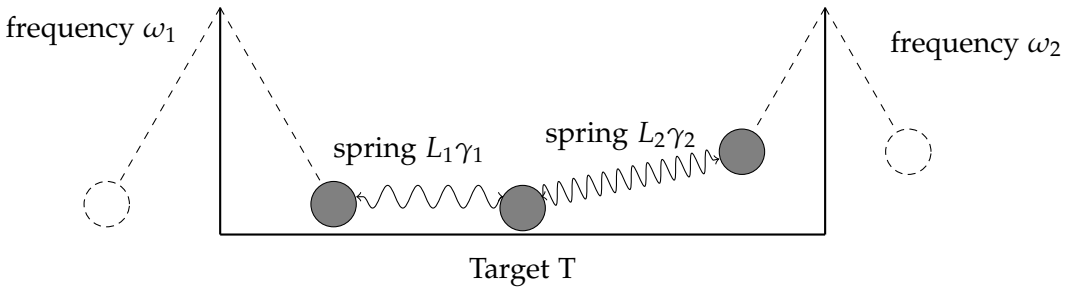

Figure 2.3.: Two pendulums at frequencies ω_1 and ω_2 connected to target T by springs representing coupling strengths $L_1\gamma_1$ and $L_2\gamma_2$

2.2. Spectral density

This spectral density of an open quantum system, e.g., a superconducting quantum bit coupled to a noisy electronic circuit, can be derived from effective friction or the noise from the environment [WKV04]. The spectral density function in this work must be anti-symmetrical due to later requirements in the decomposition process and approach zero for high frequencies as the environment only provides finite energy.

Depending on the exponential scaling factor of the frequency, spectral densities can be divided into Ohmic, Sub-Ohmic, and Super-Ohmic. Ohmic spectral densities (when the scaling factor is 1) are linearly dependent on the frequency when the frequency is low. Sub-Ohmic spectral densities (when the scaling factor is less than 1) and Super-Ohmic spectral densities (when the scaling factor is greater than 1) are non-linearly dependent on the frequency [Zha+21].

A prominent example of the Ohmic spectral density is the Debye spectral density expressed in Equation 2.4 and graphed as the green curve in Figure 2.4 with the parameters $\eta = 0.5, \gamma = 0.25$, with η resembling the coupling strength and γ representing the characteristic bath frequency.

$$S_1(\omega) = \eta \frac{\omega\gamma}{\omega^2 + \gamma^2} \tag{2.4}$$

The function's name comes from exhibiting the Debye dielectric relaxation [Wan+99] [Shi+09]. Spectral densities are usually more complicated under real-world conditions, however all general features are sufficiently captured by the Debye spectral density [Wan+99].

We introduce another Ohmic function, shown in Equation 2.5, which we later address simply as the Ohmic spectral density. The parameter Ω marks the exponential cutoff frequency [Wan+99]. We set $\Omega = 0.4$ to resemble the Debye spectral density.

$$S_2(\omega) = \pi\omega e^{-|\frac{\omega}{\Omega}|} \tag{2.5}$$

Figure 2.4.: Debye (green curve) and Ohmic (red curve) spectral densities

The function is anti-symmetrical and approaches zero for high frequencies. It is visualized in Figure 2.4 as the red curve. Compared to the exponential-cutoff of the Ohmic spectral density, the Debye spectral density has a wider frequency range, visible for $|\tau| > 2$ in Figure 2.4 [Wan+99].

2.3. Bose function

Sappler (2023) used the Bose function, as shown in Equation 2.6, to incorporate temperature in the bath correlation function [Sap23]. Le Dé et al. (2024) characterized the product of the Bose function and spectral density as the temperature-dependent spectral density [Le +24].

$$f_{Bose}(\omega) = \frac{1}{1 - e^{-\omega\beta}} \tag{2.6}$$

The inputs at $\omega_k = \frac{2\pi ik}{\beta}, k \in \mathbb{Z}$ are not defined since defining them would force a division by zero. Undefined inputs of a function are called singularities. At a singularity, a mathematical object stops behaving well by lacking analyticity or differentiability [Dim13] [FK88]. A simplified example of a singularity occurs in the reciprocal function $g(x) = \frac{1}{x}$ when $x = 0$.

2.4. Laurent expansion

Multiple expansion methods of the Bose function have been under research, a function that holds relevance in many areas of open quantum physics [HXY10].

The Laurent series builds on the Taylor series with an added singular part that includes negative exponents so that the expansion of the function approaches singularity more smoothly. Hu et al. (2010) computed the Laurent expansion of the Bose function, as seen in Equation 2.7 and 2.8, [HXY10].

$$\frac{1}{1-e^{-x}} \approx \frac{1}{x} + \frac{1}{2} + x \sum_{k=0}^{2N-1} a_k x^{2k} + \mathcal{O}(x^{4N+1}) \tag{2.7}$$

$$a_k = \frac{2k+1}{2(2k+3)!} - \sum_{j=0}^{k-1} \frac{a_1}{2k+1-2j)!} \tag{2.8}$$

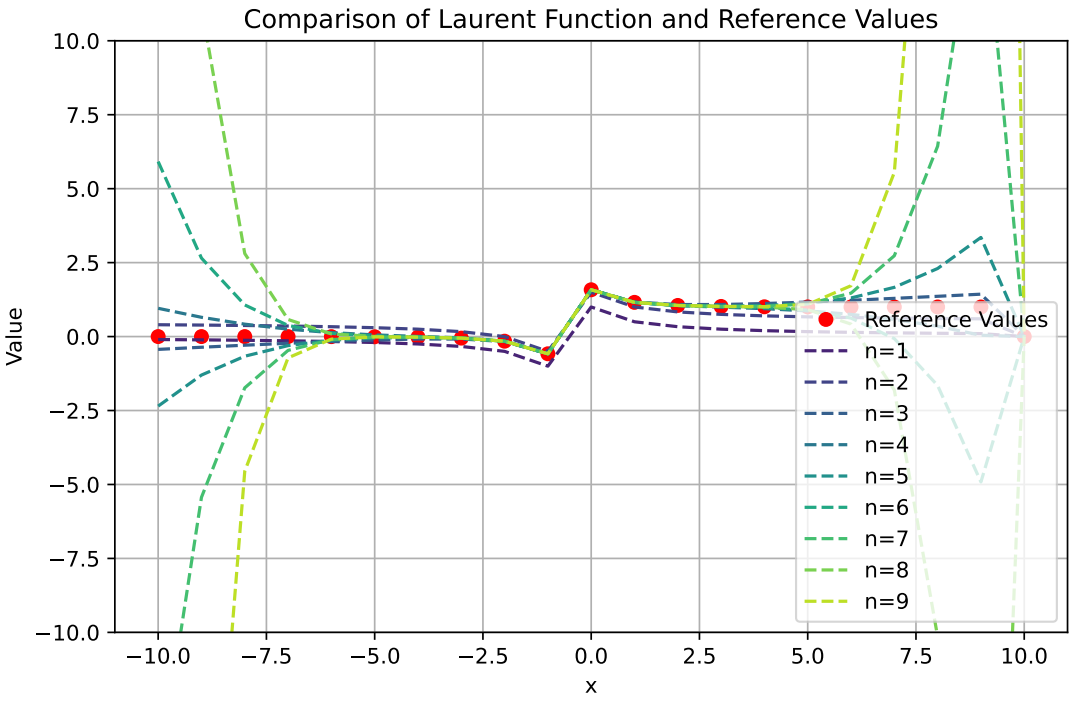

Figure 2.5.: Laurent expansion for the Bose function with increasing approximation terms n

In Figure 2.5, the graphs with more terms were drawn in brighter colors and were observed to be closer to the reference values. However, this pattern appears valid only when $|x| < 2\pi$, with the graphs no longer following the reference values outside this frame [HXY10].

We visualized the parts of the bath correlation function as building blocks of a pyramid (Figure 2.6) to provide an overview of its structure. The top building block is the spectral density, which maps the frequency of the bath mode to its energy level. We used the Fourier transform and applied the Bose function for thermal integration into the model to obtain the time-dependent correlation values of the bath.

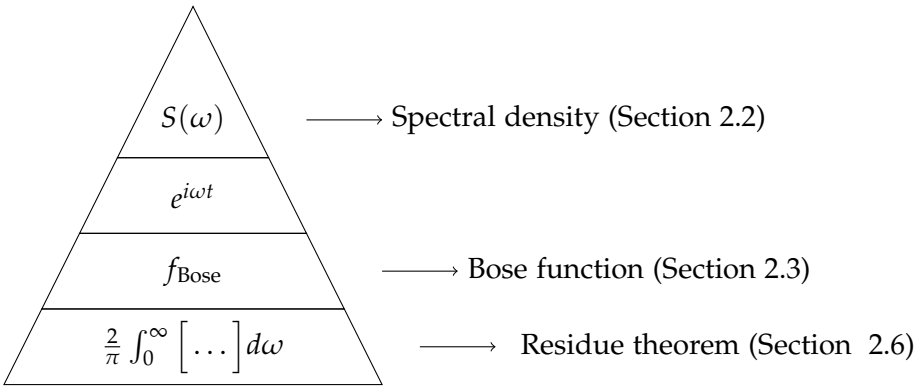

Figure 2.6.: Structure of the bath correlation function: Spectral density, Fourier transform $e^{i\omega\tau}$, Bose function, and the residue theorem with related sections in the Background

2.5. Continuum of bath modes

The bath modes on the frequency spectrum are illustrated in Figure 2.7. Three bath modes at frequencies $\omega_1, \omega_2, \omega_3$ are drawn, indicating a different energy level and coupling strength $L_k\gamma_k$ for each mode on the continuum.

The open quantum system, as seen in Figure 2.1, is now sufficiently described. The correlation values of the environment result in the bath correlation function (Equation 2.9 and [SCE15] for the derivation).

$$\alpha(\tau) = \frac{2}{\pi}\int_0^\infty S(\omega) f_{\text{Bose}} e^{i\omega\tau} \tag{2.9}$$

This integral represents a sum of limits of frequencies, but is difficult to solve analytically.

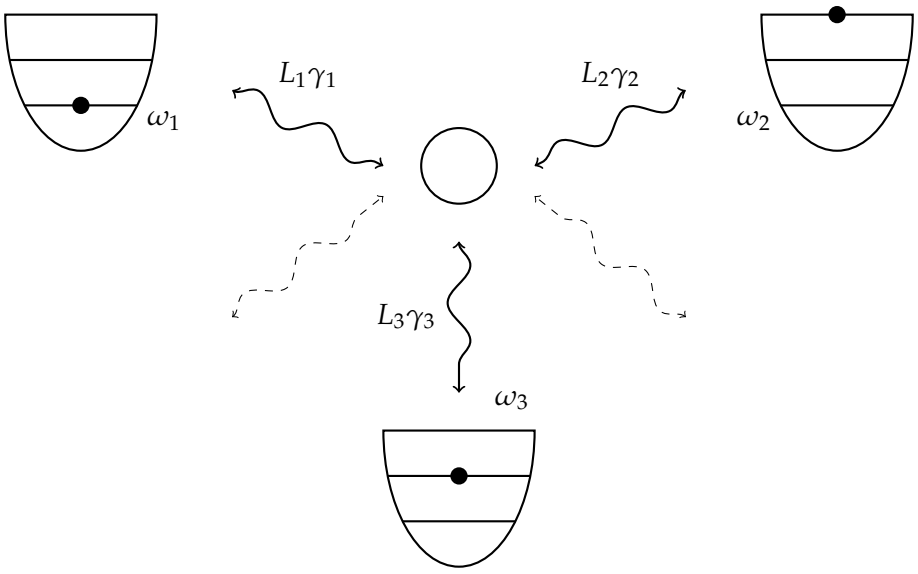

Figure 2.7.: Continuum of bath modes: Each bath mode k represents a frequency ω_k on the spectrum with coupling strength $L_k\gamma_k$

Süß et al. (2014) and other researchers used the bath correlation function represented with the hyperbolic cotangent [SES14] [Sap23] [RE14].

$$\alpha(\tau) = \frac{1}{\pi}\int_0^\infty S(\omega)\Big[\coth(\frac{\omega}{2T})\cos(\omega\tau) - i\sin(\omega\tau)\Big]dx \tag{2.10}$$

We aim to decompose the bath correlation function into a sum of exponentials, resembling Equation 2.11. Our goal is to find parameters g_k, ω_k to fit the bath correlation function. This representation holds significant benefits for subsequent methods and calculations.

$$\alpha(\tau) \approx \sum_{k=1}^{K} g_k e^{-\omega_k\tau} \tag{2.11}$$

2.6. Residue theorem

The representations of the bath correlation function (Equation 2.9 and 2.10) are mathematically challenging. Singularities can appear in the spectral density, adding further complexity. The tools to solve these challenges include the residue theorem. We extend the integral to the negative side by using the function's symmetry. Afterward, we apply the residue theorem and transform the integral into a sum.

The base for solving this integral is a mathematical path σ on which the integration occurs, as expressed in Equation 2.12. This path integral can capture points on the complex plane and integrate the function.

$$\int_{-\infty}^{\infty} f(x)dx = \int_{\sigma} f(\omega)d\omega \tag{2.12}$$

This theorem is based on the residue of a singularity. We can compute this value when approaching the singularity (Equation 2.13, Fischer & Kaul, p.566) [FK88]. We examine the function $g(z)$ inside an integral with singularities at points z_k.

$$\mathrm{Res}(g, z_k) = \lim_{z \to z_k} (z - z_k)g(z) \tag{2.13}$$

The integral can be evaluated by constructing a large path on the real axis, as shown in Figure 2.8. This path approaches negative and positive infinity on each end of the axis. The limits are abstracted to a respective endpoint, which connects to the axis to form a semicircle in the complex plane [FK88].

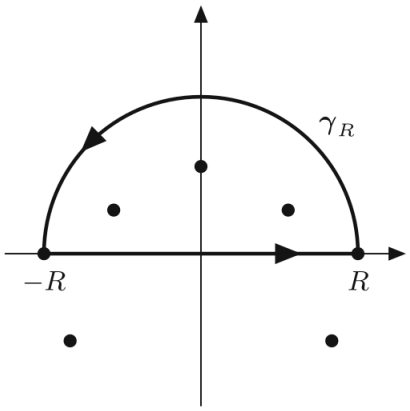

Figure 2.8.: Schematic representation of the residue theorem: Imaginary singularities are black dots and path integral is represented by the black semi-circle (Fischer & Kaul, p.570) [FK88]

The theorem transforms the integral into the sum of all residue in the region enclosed by the semicircle. We apply the residue theorem to the bath correlation function, which results in Equation 2.14.

$$\alpha(\tau) = \frac{1}{\pi} \int_{-\infty}^{\infty} S(\omega) f_{\mathrm{Bose}} e^{i\omega\tau} dx = \frac{1}{\pi} \left[2\pi i \sum_{k=1}^{\infty} \mathrm{Res}(z_k) \right] \tag{2.14}$$

We present a thought experiment for this theorem with Figure 2.9. The grey surface on the left resembles a landscape with various dips and curves. Above the surface, two green watering cans are pouring water onto it. The surface has different regions with multiple colors, indicating variations in height across the surface. The image symbolizes a system receiving inputs (the water inflow) into a complex environment (the wavy surface) and outputs (the water outflow).

On the right, the mathematical function is plotted.

$$f(x) = \frac{1}{(x+15)^2} + -\frac{1}{(x+7)^2} - \frac{1}{x^2} + \frac{1}{(x-4)^2} \tag{2.15}$$

It has four singularities at $z_i \in \{-15, -7, 0, 4\}$. The watering cans and surface on the left are an analogy for the graph with poles. The residue theorem can determine the landscape by taking the poles into account. We keep in mind that the residue theorem is based on imaginary poles, which is not considered in this analogy.

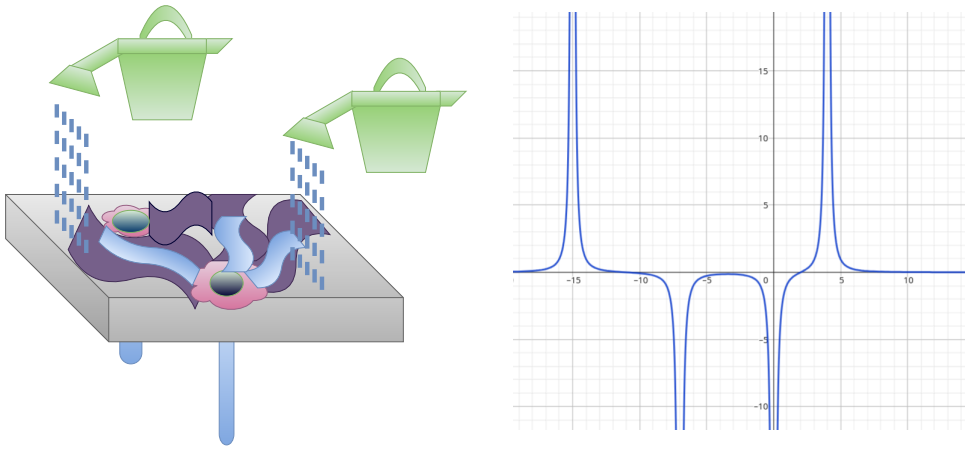

Figure 2.9.: Analogy for the residue theorem

3. Related Work

Numerous studies have extensively explored the bath correlation function, which is crucial in understanding the dynamics of open quantum systems. In the following, we provide a non-exhaustive overview of associated research, mainly focusing on the exponential sum decomposition as illustrated in Equation 2.11.

3.1. Exponential sum decomposition

In 2014, the bath correlation function was expressed as a sum of damped harmonic oscillators to a given spectral density by Ritschel & Eisfeld (2014) [RE14]. The authors expanded the hyperbolic cotangent, rather than the Bose function, using the alternative representation of the bath correlation function, presented in Equation 2.10. Additionally, they used the residue theorem, analogous to Equation 2.14, to generate the exponential sum. This decomposition is crucial, as multiple numerical methods describing open quantum systems require the bath correlation function in this form [RE14]. The sum of exponentials is further beneficial as relevant spectral distribution can be fitted to this form [DPW12].

3.2. Methods based on the exponential sum decomposition

Dattani et al. (2012) provided an overview of calculations in which this decomposition is useful [DPW12]. Namely the Nakajima-Zwanzig equation [SV10], the Hierarchical Equations of Motion (HEOM) [Tan90] and the Non-Markovian Quantum state Diffusion- Zeroth Order Functional Expansion (NMQSD-ZOFE) Quantum Master Equation [Rit+11].

The Hierarchical Equations of Motion is a leading method for analyzing open quantum systems and continues to be the subject of extensive scientific investigation [Fay22] [Cui+20]. Xu & Yan (2007) constructed a formalism based on a calculus-on-path-integral algorithm [XY07] and Ke et al. (2022) used a twin-space formulation of the hierarchical equations of motion approach in combination with matrix product state representation [KBT22].

In a different approach, Süß et al. (2014) used stochastic evolution equations for quantum trajectories and applied them to the spin-boson model [SES14]. They also expanded the hyperbolic cotangent like [RE14] with a Padé expansion. Following that, Sappler (2023) implemented the Hierarchy of Pure States and the Hierarchy of Matrix Product States and calculated the Matsubara frequencies for the Debye spectral density [Sap23]. Matsubara frequencies represent the method of a closed bath correlation applied to the residue theorem.

3.3. Bath correlation function

The bath correlation function eventually determines the influence of the environment on the system [SCE15]. This fundamental influence results in a wide range of applications and a long history of research. Breton et al. (1984) studied different relaxations of a quantum system and determined relaxation super-operators with the bath correlation function [Bre+84]. De Boeij et al. (1996) derived the bath correlation function from conventional and time-gated stimulated photon echo experiments [BPW96]. Strümpfer & Schulten (2011) integrated the bath correlation function in their research about photosynthesis [SS11]. Schönleber et al. (2015) constructed so-called pseudomodes into the bath and integrated a temperature-dependent bath correlation function [SCE15].

3.4. Spin-boson model

The spin-boson model describes the open quantum system shown in Figure 2.1. This model is the simplest nonlinear system, which includes the interaction of quantum coherence and thermal fluctuations and has a wide range of applications [Wei12].

In 1994, the spin-boson model was applied to characterize the coupling between protein motion and electron transfer in the photosynthetic reaction center by Xu & Schulten (1994) [XS94]. Gilmore & McKenzie (2006) inspected the Förster resonant energy transfer between two optically active molecules, described by a spin-boson model [GM06].

3.5. This work's objective

To conclude this overview, the introduced concepts in the background strongly interest the science community. We acknowledge that exponential sum decomposition methods achieve strong relevancy. In the latter, we aim to decompose the bath correlation function using methods including residue theorem and Laurent expansion.

4. Results

We decompose the bath correlation function, see Equation 2.9, in multiple steps, in which we face mathematical challenges. The structure of the function, visualized as a pyramid in Figure 2.6, is extended by three main research areas in Figure 4.1. Initially, a numerical reference framework is provided to validate our results, followed by applying the residue theorem. This theorem supports the decomposition process by providing a way to solve challenging integrals. We then expand the Bose function, which allows us to express the Bose function as an infinite sum. Finally, we test our procedure with the Ohmic spectral density.

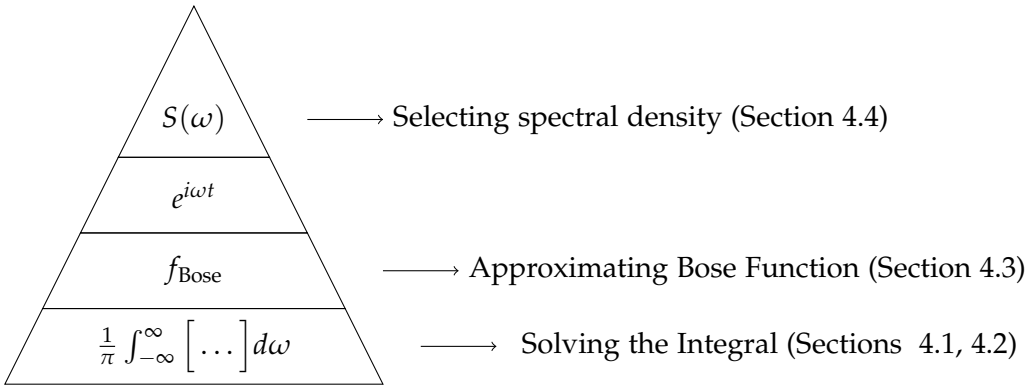

Figure 4.1.: Pyramid structure of the bath correlation function with respective sections

4.1. Numerical validation framework

We build a consistent framework to keep the decomposition results in check and rely on numerical approximation. This approximation focuses on validation, and numerical accuracy is of minor priority. The design of this framework includes reduced computational resources and fast run times. We use Equation 2.9 with Debye Spectral density and apply the general integration approach from the SciPi [Sci24] library.

We split the integral, see Equation 2.9, as we approach a singularity at $\omega = 0$. a, b are

lower and upper integration limits and ϵ denotes the distance to the singularity.

$$\alpha(\tau) = \frac{1}{\pi}\int_{-\infty}^{\infty} S(\omega) f_{Bose} e^{i\omega\tau} d\omega \approx \frac{1}{\pi}\Big[\int_{a}^{-\epsilon} S(\omega) f_{Bose} e^{i\omega\tau} d\omega + \int_{\epsilon}^{b} S(\omega) f_{Bose} e^{i\omega\tau} d\omega\Big] \tag{4.1}$$

These integration limits and the distance to the singularity are evaluated in Figure 4.2.

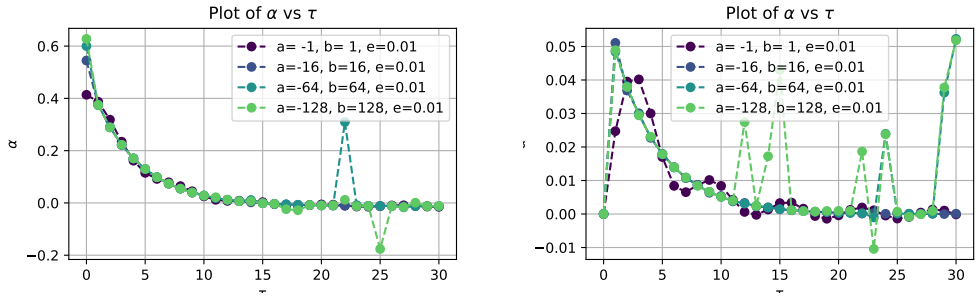

Figure 4.2.: Real and imaginary part: Comparing integral limits

The significant share of the integral lies near zero as both real and imaginary curves, see Figures 4.2, between $a = -1, b = 1$ incorporate many characteristics from curves with higher integration limits. For the real part, in Figure 4.2, we acknowledge numerical irregularities with limits greater than $|a| > 16$. These irregularities are flagged as an 'Integration Warning' by the library function, indicating potential issues with the accuracy of the integration. The imaginary plot displays further approximation errors within higher limits. We base our limits on $a = -16, b = 16$ to minimize these irregularities and still have a steady curve compared to smaller limits.

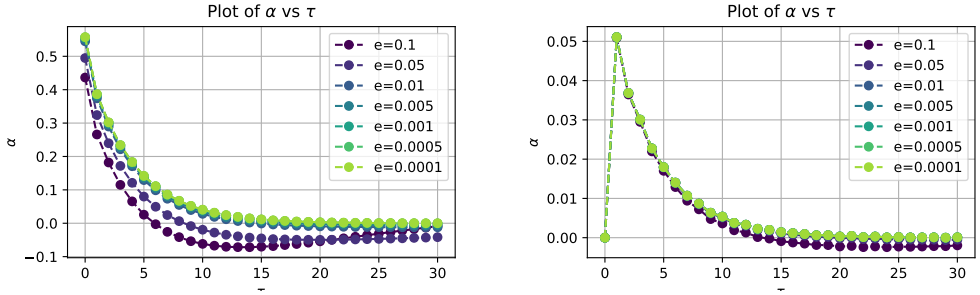

Figure 4.3.: Real and imaginary part: Distance to singularity

We approach this singularity with different distances ϵ in Figures 4.3. These Figures indicate that the area around zero is significant for evaluating the integral. The real

distance to the singularity impacts the resulting integral. Still, for smaller distances, the difference gets less relevant. We apply $\epsilon = 0.01$ as a trade-off between accuracy and practicality.

4.2. Utilizing the residue theorem

The residue theorem disassembles the function as the characteristics of the function make the integration hard to solve. The real-valued integral over complex numbers is transformed into the integral over a complex path and further into a sum of exponentials supported by the residue theorem, as shown in Equation 2.14 in the Background. We derived this decomposition for the Debye spectral density in Appendix A.1 Equation A.30.

$$\alpha_{\text{Debye}}(\tau) \approx \eta i\gamma \frac{1}{1 - e^{-i\gamma\beta}} e^{-\gamma\tau} + \sum_{k=1}^{K} \eta \frac{(4\pi k T \gamma)}{(4\pi^2 k^2 T^2 + \gamma^2)} e^{-2\pi k \tau} \tag{4.2}$$

We insert the parameters $\eta = 0.5, \gamma = 0.25, T = 1, K = 5$, [SES14] [Sap23] and compare it with general purpose integration approximation. We present the real part of this decomposition. We use the residue theorem and take the singularity $z_0 = i\gamma$ and $z_k = 2\pi ik$ into account.

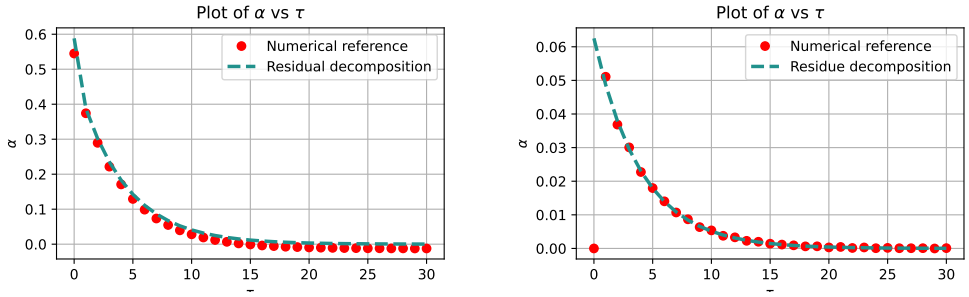

Figure 4.4.: Real and imaginary part: Compare numerical reference with residue decomposition

The residue decomposition successfully approximates the bath correlation function. The correlation values $\alpha(\tau)$ declines for higher time intervals τ, see Figure 4.4. Values smaller than zero appear, which is impossible for the residues as the e function only approaches and never passes zero. To enhance visibility, we plot the absolute error in a logarithmic scale in Figure 4.5. The error rates to the numerical approximation are, in general, minimal.

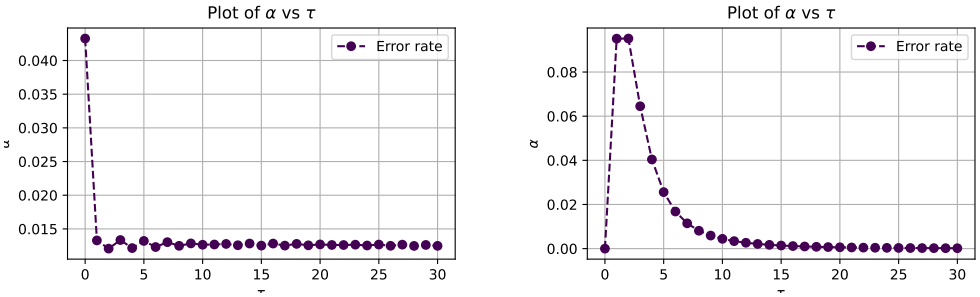

Figure 4.5.: Real and imaginary part: Error rates of the residue decomposition

We spitted the first four terms of the exponential sum (Equation 4.2) and plotted the significance of the individual terms of the exponential sum.

Term	Expression
$k = 0$	$\eta i\gamma \frac{1}{1-e^{-i\gamma\beta}} e^{-\gamma\tau}$
$k = 1$	$\eta \frac{(4\pi T\gamma)}{(4\pi^2 T^2+\gamma^2)} e^{-2\pi\tau}$
$k = 2$	$\eta \frac{(8\pi T\gamma)}{(16\pi^2 T^2+\gamma^2)} e^{-4\pi\tau}$
$k = 3$	$\eta \frac{(12\pi T\gamma)}{(36\pi^2 T^2+\gamma^2)} e^{-6\pi\tau}$
$k = 4$	$\eta \frac{(16\pi T\gamma)}{(64\pi^2 T^2+\gamma^2)} e^{-8\pi\tau}$

Table 4.1.: First four terms of the expansion of $\alpha_{\text{Debye}}(\tau)$ for $k = 0$ to $k = 4$.

As shown in Figure 4.6, the first term ($k = 0$ in purple) is exclusively responsible for the accuracy of the decomposition. The remaining terms of the sum do not sufficiently influence the integral.

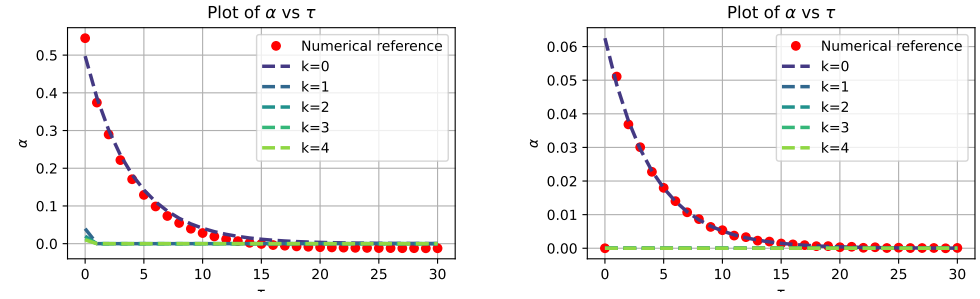

Figure 4.6.: Influences of terms: Real and Imaginary Part

We gathered information about the importance of the terms that lead to the final result

with α_{num} as the numerical reference and t_k the kth term of the decomposition—starting with k_0 as the leading term.

$$p_k = \left| 1 - \frac{\alpha_k - \alpha_{\text{num}}}{\alpha_{\text{num}}} \right| \tag{4.3}$$

leading to Figure 4.7. p_k denotes the ratio between the numerical reference value α_{num} and the kth term α_k. The first term has noticeably more impact than the other terms, as it accounts for over 80% of the reference value for $\tau < 5$, as shown in Figure 4.7.

The first term ($k = 0$) originates from the singularity of the spectral density. However, certain spectral density do not exhibit imaginary singularities (see Equation A.67) and their decomposition might only rely on the singularities of the Bose function. That might lead to a comparable minimal impact and reduced accuracy of the decomposition.

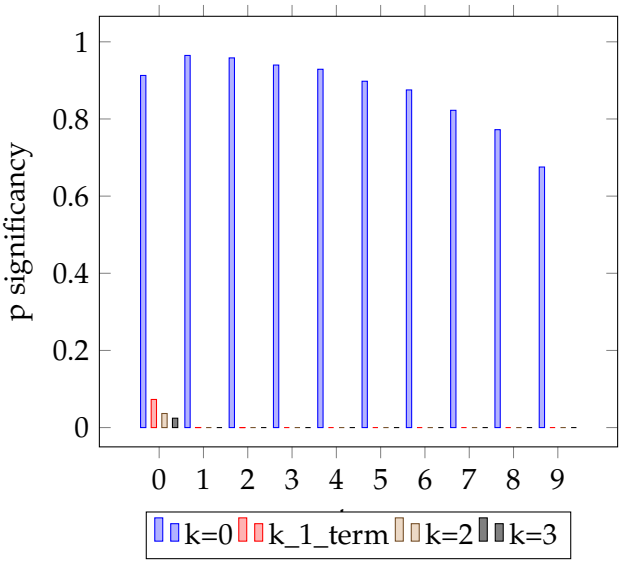

Figure 4.7.: Column diagram of the four data series

We conclude that the singularity $z = i\gamma$ originating from the Debye spectral density is the central aspect of the decomposition. The remaining singularities (of the Bose function) do not appear relevant for the decomposition in this parameter configuration, at least for $T = 1$.

4.3. Laurent expansion

In the next step, we examine the Laurent expansions for the Bose function. As mentioned in the Background, the Bose function is a prominent function in quantum physics and has been profoundly researched [HXY10]. We use the Laurent series to express the Bose function more compactly. As seen in the Background, only a few terms are enough to yield a decent approximation of the original Bose function. We choose $N = 2$ as a sufficient approximation.

$$f_{Bose}(\omega\beta) = \frac{1}{1 - e^{-\omega\beta}} \approx \frac{1}{x} + \frac{1}{2} \tag{4.4}$$

As seen in the appendix A.2, we derived the exponential sum decomposition:

$$\alpha(\tau) = \left[\frac{\eta}{\beta} + i\eta\frac{\gamma}{2}\right] e^{-\gamma\tau} \tag{4.5}$$

The numerical approximation with the Bose function (Figure 2.5) is accurate with the Laurent approximation. Still, it is only a minor focus as it does not provide more insights to decompose into a sum of exponentials.

Figure 4.8 shows the Laurent expansion approximating the bath function correlation function. Further research could also look into Padé expansion [Sap23] as potentially more singularities are available for the residue theorem. The imaginary part in Figure 4.8 appears accurate.

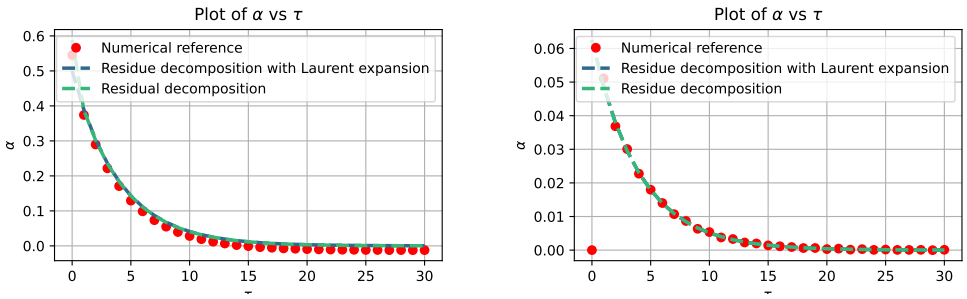

Figure 4.8.: Real and imaginary part: Compare numerical reference with Laurent expansions

This approximation is relatively sophisticated, as depicted in Figure 2.5. The green curve represents the decomposition with an expanded Bose function.

4.4. Ohmic spectral density

The function, as shown in Equation 2.5, is transformed with the residue theorem into a sum of exponentials, see Appendix A.3 and Equation A.67:

$$\alpha(\tau) \approx -4\pi^2 \sum_{k=1}^{K} k e^{-2\pi k T(\frac{1}{\Omega}+\tau)} \tag{4.6}$$

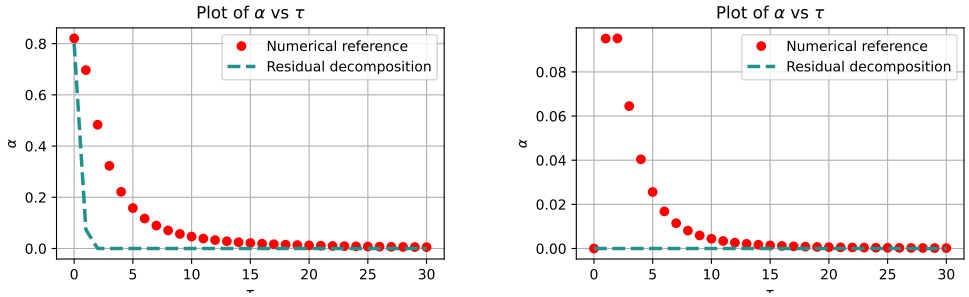

Figure 4.9.: Real and imaginary part: Compare numerical reference with residue decomposition

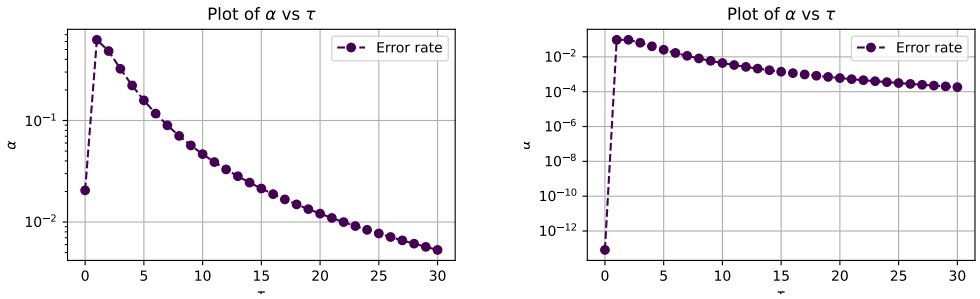

Figure 4.10.: Real and imaginary part: Error rates of the residue decomposition

We insert the parameters $\Omega = 0.4, T = 1$. In Figure 4.9, the residue curve immediately drops to zero, and the imaginary curve is indifferent from zero, which is also supported by the error plots in Figure 4.10. They display the deviations on a logarithmic scale. There are deviations from up to 0.6 at the start, which resembles nearly the numerical reference value. The decomposition follows the same trend but can not be seen as a meaningful approximation.

It's important to note that the Ohmic spectral density does not show singularities on the imaginary axis. Therefore, the residue theorem depends on the Bose function's

singularities. As we saw with the debye decomposition, these singularities have nearly no influence on the integral. The Ohmic spectral density with no own imaginary singularities is challenging to decompose with this method.

4.5. Comparing different temperature regimes

We broaden our hypothesis by applying a more comprehensive range of temperatures to decompositions. We selected four temperature configurations: $T \in \{0.02, 0.5, 2, 5\}$ as we already covered $T = 1$. Brighter colors in green represent smaller temperatures, and darker reds represent smaller temperatures in the numerical reference.

4.5.1. Debye spectral density

For the Debye spectral density, we use $\eta = 0.5, \gamma = 0.25, K = 5$. In Figure 4.12 (next page), all the temperature curves are accurately decomposed except for the low-temperature $T = 0.02$. The imaginary curve is accurate and unchanged for different temperatures.

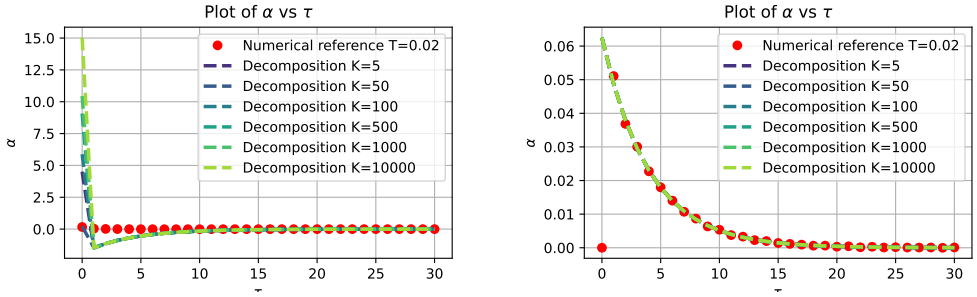

Figure 4.11.: Temperature Comparison for Debye spectral density: Real and Imaginary Part

Figure 4.11 shows increasing decomposition terms for temperature $T = 0.02$. Sapper (2023) applied more approximation terms to fix the decomposition at $T = 0.02$ and achieve meaningful approximation at $K = 1000$ [Sap23]. However, this result could not be replicated with our model. We used different numbers of approximation terms $K \in \{5, 50, 100, 500, 1000, 10000\}$.

Figure 4.11 illustrates no meaningful approximation for $T = 0.02$ with increasing approximation terms. We observed a rise in the initial value up to $\alpha(0) \approx 15.029$ for $K = 10000$. As for $K = 5$ in Figure 4.12, the imaginary curve is sufficiently approximated by the decomposition.

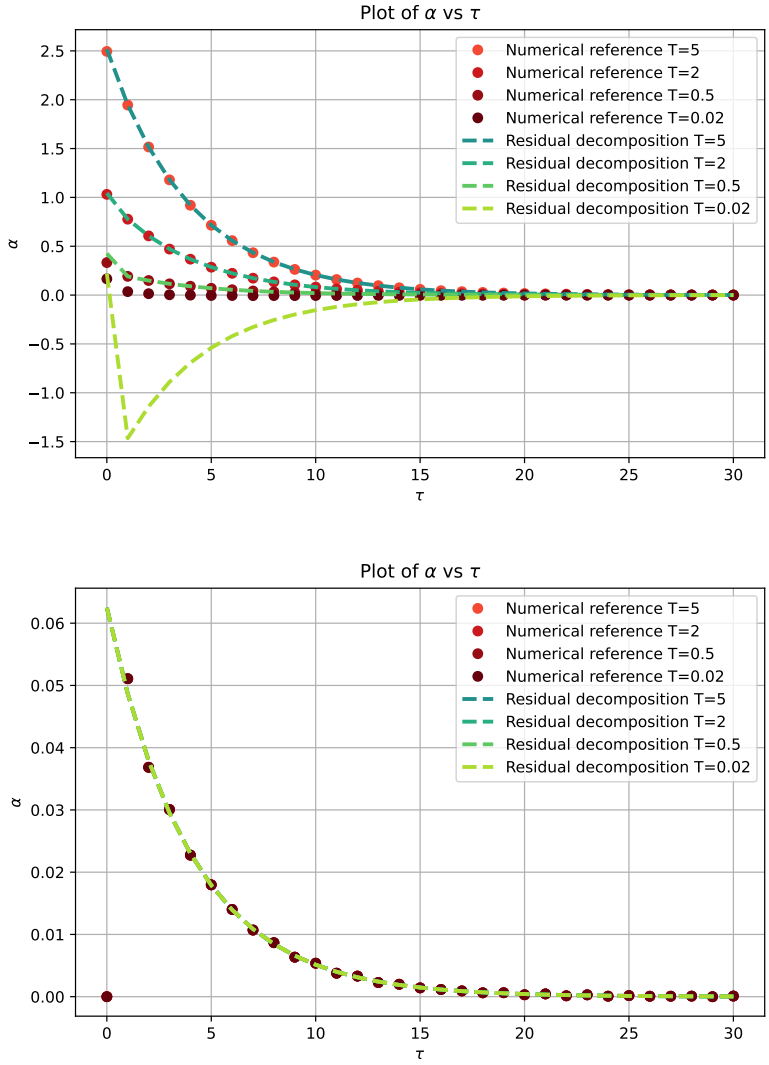

Figure 4.12.: Temperature Comparison for Debye spectral density: Real and Imaginary Part

4.5.2. Ohmic spectral density

In the numerical validation framework for $T = 0.02$, we encountered a 'RuntimeWarning' for the Ohmic decomposition. An overflow for 'return 1/(1-numpy.exp(-x/T))' is flagged, which highlights that numerical integration are prone to numerical errors, and the need for a fast and accurate decomposition is emphasized.

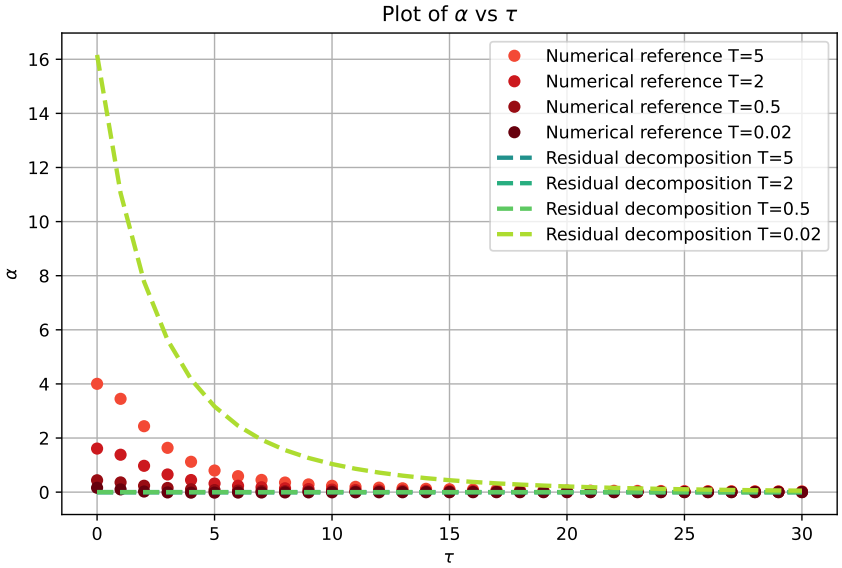

Figure 4.13.: Temperature Comparison for Ohmic spectral density: Real and Imaginary Part

For the Ohmic spectral density decomposition, we use $\Omega = 0.4, K = 5$. All real curves in high-temperature areas are close to zero. The curve for $T = 0.02$ stabilizes and has extremely high values ($\alpha(0) \approx 16.161$). However, none of the curves provides a meaningful decomposition. We could not compare the imaginary values of the decompositions as Equation 4.6 has no imaginary part.

5. Discussion

We exhaustively examine selected parameters, values, and meta-information to identify connections or errors that might compromise the accuracy and validity of our data. We plotted τ between 0 and 30 and with step size 1, following [Sap23]. Possible errors include integration of the parameters, the residue calculation, the residue proof chain, or errors in the implementation.

5.1. Numerical reference framework

The numerical reference framework is not exhaustively accurate, as the framework compares the overall trend of the bath correlation function and validates the residues on a broad scale while maintaining fast run times. As of the symmetric properties of the integral, the positive part would have serviced for our calculations.

We used the general purpose integration (quad) of the SciPi library [Sci24]. This library provides fast results and integrates the time parameter in the integral. There are other possible modes of integration, e.g., the equispaced sampling technique by Romberg or the arbitrary spacing with the Simpson rule [Sci24].

The limits are chosen at $a = -16, b = 16$ because of sufficient accuracy in approximation and numerical errors at higher limits. The library function includes an option for limits at -∞, $+\infty$ to make it as accurate as possible, which was unnecessary in our case. The numerical framework validates trends of the decomposition with the residue theorem.

5.2. Residue theorem

The main property of the decomposition is the number of approximation terms in usage. Research has shown that this decomposition method is more applicable to higher frequencies [MT99], which we could replicate in Figure 4.12. We used a limited number of $K = 5$ terms, but we increased the approximation terms for low-temperature applications. The added terms did not increase the accuracy of the decomposition as expected, and potential errors in the implementation of the calculations can be subject to future work. The main result of our analysis is that the result of the decomposition

relies heavily on the first term, as over 80% of the numerical reference value was covered by the first term for the Debye spectral density at $T = 1$ as for the first $\tau = 5$ time steps.

The Ohmic spectral density, which does not rely on an imaginary singularity, was not decomposed successfully. The numerical framework showed massive deviations.

5.3. Parameters of spectral densities

We instantiated Ohmic and Debye spectral density with the parameter $\eta = 0.5, \gamma = 0.25$ for the Debye spectral density. Prior research relied on these values [Sap23] [SES14].

We chose parameter $\Omega = 0.4$ for the Ohmic spectral density to resemble the curve of the Debye spectral density in order to achieve a consistent comparison. In comparison, the Debye spectral density spans a broader range in frequencies than the Ohmic. However, their trend is similar [Wan+99]. Parameters for temperature were tested primarily for $T = 1$ and in the latter for a range of low to high temperatures ($T = 0.02$ to $T = 5$) with difficulties in the low-temperature regime.

5.4. Laurent expansion

The Laurent series successfully expands the Bose function. We are using $N = 2$ terms for the approximation, sufficient to expand the Bose function. These series expansions can be further applied using different methods. Other research was focused on expanding the hyperbolic cotangent [SES14]. A possible future work would be to find an expansion for the temperature-dependent spectral density—the combination of spectral density and Bose function [Le +24]. Further possible expansions include the Padé and Fano expansions, which aim to solve the difficulties in low-temperature regimes [HXY10] [Le +24].

6. Conclusion

We tested decomposition methods for the bath correlation function, including the residue theorem and the Laurent series expansion. We applied the often-used Debye spectral density and a newly constructed Ohmic spectral density, which had resembling characteristics. We compared these with the numerical general-purpose integration, and the results were accurate for the Debye spectral density. The method was not successful for the Ohmic spectral density. The the data shows an apparent deviation in all temperature ranges. The Laurent series expansion had similar results for the Debye spectral density. The series expansion could be further verified in future work with more spectral densities and more advanced expansion methods. We suggest assessing spectral density with larger differences to assess the behavior of the bath correlation function.

A. Residue theorem

This appendix contains supplementary material, such as detailed derivations and calculations on the residue theorem.

As the residue theorem operates on integral from $-\infty$ to $+\infty$, the bath correlation function is extended to the complete real axis. We make use of its symmetric properties and transform into Equation A.2:

$$\alpha(\tau) = \frac{2}{\pi}\int_0^\infty S(\omega) f_{\text{Bose}}(\omega\beta) e^{i\omega\tau} d\omega \tag{A.1}$$

$$\alpha(\tau) = \frac{1}{\pi}\int_{-\infty}^\infty S(\omega) f_{\text{Bose}}(\omega\beta) e^{i\omega\tau} d\omega \tag{A.2}$$

A.1. Derivation for the Debye spectral density

$$\alpha(\tau) = \frac{1}{\pi}\int_{-\infty}^\infty \eta \frac{\omega\gamma}{\omega^2+\gamma^2}\frac{1}{1-e^{-\omega\beta}} e^{i\omega\tau} d\omega \tag{A.3}$$

$$g(\omega) = \eta \frac{\omega\gamma}{\omega^2+\gamma^2}\frac{1}{1-e^{-\omega\beta}} e^{i\omega\tau} \tag{A.4}$$

The residue theorem is applied with these residues $z_0 = i\gamma$ $z_k = 2\pi i k T$, $k \in \mathbb{N}^+$ The function inside the integral is expressed as:

$$\int_{-\infty}^\infty \eta \frac{\omega\gamma}{\omega^2+\gamma^2}\frac{1}{1-e^{-\omega\beta}} e^{i\omega\tau} d\omega = 2\pi i \sum_{\Im(z_k)>0} \text{Res}(g, z_k) \tag{A.5}$$

$$= 2\pi i \Big[\text{Res}(g, i) + \sum_{k=0}^{\infty} \text{Res}(g, 2\pi i k T)\Big] \tag{A.6}$$

A.1.1. Residuum at $i\gamma$

Using $0 \neq \gamma \in \mathbb{R} \setminus \mathbb{C}$ in the following:

The residue of the function $g(z)$ at z_0 is given by, (Fischer & Kaul, p.566) [FK88] :

$$\text{Res}(g(z), z_0) = \lim_{z\to z_0} (z - z_0) g(z) \tag{A.7}$$

First, simplify by noting that $(z - i\gamma)$ can be left out:

$$\text{Res}(g, i\gamma) = \lim_{z \to i\gamma} \eta \frac{z\gamma}{(z + i\gamma)} \frac{1}{1 - e^{-z\beta}} e^{iz\tau} \tag{A.8}$$

Since $e^{-\gamma} \neq 1$, there is no additional singularity from $\frac{1}{1-e^{-z\beta}}$.
Substitute $z = i\gamma$ into the expression:

$$\text{Res}(g, i\gamma) = \eta \frac{(i\gamma)\gamma}{(i\gamma + i\gamma)} \frac{1}{1 - e^{-i\gamma\beta}} e^{i(i\gamma)\tau} \tag{A.9}$$

Simplify the expression:

$$\text{Res}(g, i\gamma) = \eta \frac{i\gamma^2}{2i\gamma} \frac{1}{1 - e^{-i\gamma\beta}} e^{-\gamma\tau} \tag{A.10}$$

Thus, the residue is:

$$\text{Res}(g, i\gamma) = \eta \frac{\gamma}{2} \frac{1}{1 - e^{-i\gamma\beta}} e^{-\gamma\tau} \tag{A.11}$$

A.1.2. Residuum at $z_k = 2\pi ik$

The residue of $g(z)$ at z_k is given by:

$$\text{Res}(g, z_k) = \lim_{z \to z_k} (z - z_k) g(z) \tag{A.12}$$

Substitute $z_k = 2\pi ikT$:

$$\text{Res}(g, z_k) = \lim_{z \to 2\pi ikT} (z - 2\pi ikT) \eta \frac{z\gamma}{z^2 + \gamma^2} \frac{1}{1 - e^{-z\beta}} e^{iz\tau} \tag{A.13}$$

Rearrange:

$$= \lim_{z \to 2\pi ikT} \eta \frac{z\gamma}{(z - i\gamma)(z + i\gamma)} \frac{(z - 2\pi ikT)}{1 - e^{-z\beta}} e^{iz\tau} \tag{A.14}$$

We split the limes, as they are both converging (Fischer & Kaul, p.164) [FK88]

$$= \lim_{z \to 2\pi ikT} \eta \frac{z\gamma}{(z - i\gamma)(z + i\gamma)} e^{iz\tau} \lim_{z \to 2\pi ikT} \frac{(z - 2\pi ikT)}{1 - e^{-z\beta}} \tag{A.15}$$

Apply de l'Hospital derivation rule on the second limes, (Fischer & Kaul, p.195) [FK88]

$$= \lim_{z \to 2\pi ikT} \eta \frac{z\gamma}{(z - i\gamma)(z + i\gamma)} e^{iz\tau} \lim_{z \to 2\pi ikT} \frac{\frac{d}{dz}(z - 2\pi ikT)}{\frac{d}{dz}(1 - e^{-z\beta})} \tag{A.16}$$

Take the derivative:

$$= \lim_{z \to 2\pi ikT} \eta \frac{z\gamma}{(z - i\gamma)(z + i\gamma)} e^{iz\tau} \lim_{z \to 2\pi ikT} \frac{1}{e^{-z\beta}} \tag{A.17}$$

As $\gamma \neq 2\pi ikT$, substitute the value in both limes:

$$= \eta \frac{(2\pi ikT)\gamma}{(2\pi ik - i\gamma)(2\pi ikT + i\gamma)} \frac{1}{e^{-(2\pi ikT)\beta}} e^{i(2\pi ikT)\tau} \tag{A.18}$$

Transform:

$$= \eta \frac{(2\pi ik)\gamma}{(2\pi ik)^2 - \gamma^2} \frac{1}{e^{-(2\pi ik)}} e^{-2\pi kT\tau} \tag{A.19}$$

Since $e^{-2\pi ikT\beta} = 1$:

$$= \eta \frac{(2\pi ik)\gamma}{(2\pi ikT)^2 - \gamma^2} e^{-2\pi kT\tau} \tag{A.20}$$

Multiply the parentheses:

$$= \eta \frac{2\pi ikT\gamma}{4\pi^2 i^2 k^2 T^2 - \gamma^2} e^{-2\pi k\tau} \tag{A.21}$$

Get out the -1

$$= \eta \frac{2\pi ikT\gamma}{-4\pi^2 k^2 T^2 - \gamma^2} e^{-2\pi k\tau} \tag{A.22}$$

$$= \eta \frac{2\pi ikT\gamma}{-(4\pi^2 k^2 T^2 + \gamma^2)} e^{-2\pi k\tau} \tag{A.23}$$

Combine the terms:

$$\alpha(\tau) = \frac{1}{\pi} 2\pi i \left[\mathrm{Res}(g, z_0) + \sum_{k=1}^{\infty} \mathrm{Res}(g, z_k) \right] \tag{A.24}$$

Substitute:

$$= 2i \left[\eta \frac{\gamma}{2} \frac{1}{1 - e^{-i\gamma\beta}} e^{-\gamma\tau} + \sum_{k=1}^{\infty} \eta \frac{2\pi ikT\gamma}{-(4\pi^2 k^2 T^2 + \gamma^2)} e^{-2\pi k\tau} \right] \tag{A.25}$$

Multiply factors $2i$ inside:

$$= \left[\eta i\gamma \frac{1}{1 - e^{-i\gamma\beta}} e^{-\gamma\tau} + \sum_{k=1}^{\infty} \eta \frac{4\pi i^2 kT\gamma}{-(4\pi^2 k^2 T^2 + \gamma^2)} e^{-2\pi k\tau} \right] \tag{A.26}$$

Since $i^2 = -1$:

$$= \left[\eta i\gamma \frac{1}{1 - e^{-i\gamma\beta}} e^{-\gamma\tau} + \sum_{k=1}^{\infty} \eta \frac{-(4\pi kT\gamma)}{-(4\pi^2 k^2 T^2 + \gamma^2)} e^{-2\pi k\tau} \right] \tag{A.27}$$

Simplify:

$$= \eta i\gamma \frac{1}{1 - e^{-i\gamma\beta}} e^{-\gamma\tau} + \sum_{k=1}^{\infty} \eta \frac{(4\pi kT\gamma)}{(4\pi^2 k^2 T^2 + \gamma^2)} e^{-2\pi k\tau} \tag{A.28}$$

$$\alpha(\tau) = i\eta\gamma \frac{1}{1 - e^{-i\gamma}} e^{-\gamma\tau} + \sum_{k=1}^{\infty} \eta \frac{4\pi k\gamma}{4\pi^2 k^2 + \gamma^2} e^{-2\pi k\tau} \tag{A.29}$$

We only apply limited approximation terms K:

$$\alpha(\tau) = i\eta\gamma \frac{1}{1 - e^{-i\gamma}} e^{-\gamma\tau} + \sum_{k=1}^{K} \eta \frac{4\pi k\gamma}{4\pi^2 k^2 + \gamma^2} e^{-2\pi k\tau} \tag{A.30}$$

A.2. Derivation for the Debye spectral density with Laurent expansion

$$\alpha(\tau) = \frac{1}{2\pi} \int_0^{\infty} S(\omega) \Big[\frac{1}{\omega\beta} + \frac{1}{2} \Big] e^{i\omega\tau} d\omega \tag{A.31}$$

After the transformations from [Sap23]:

$$\alpha(\tau) = \frac{1}{\pi} \int_{-\infty}^{\infty} S(\omega) \Big[\frac{1}{\omega\beta} + \frac{1}{2} \Big] e^{i\omega\tau} d\omega \tag{A.32}$$

$$\alpha(\tau) = \frac{1}{\pi} \int_{-\infty}^{\infty} \eta \frac{\omega\gamma}{\omega^2 + \gamma^2} \Big[\frac{1}{\omega\beta} + \frac{1}{2} \Big] e^{i\omega\tau} d\omega \tag{A.33}$$

$$g(\omega) = \eta \frac{\omega\gamma}{\omega^2 + \gamma^2} \Big[\frac{1}{\omega\beta} + \frac{1}{2} \Big] e^{i\omega\tau} \tag{A.34}$$

$T = 1$ $z_0 = i\gamma$ $z_k = 2\pi ik, k \in \{1, 2, 3 \dots\}$

We now take the residue theorem, which is the same as the extended integral

$$\int_{-\infty}^{\infty} \eta \frac{\omega\gamma}{\omega^2 + \gamma^2} \Big[\frac{1}{\omega\beta} + \frac{1}{2} \Big] e^{i\omega\tau} d\omega = 2\pi i \sum_{\Im(z_k) > 0} \mathrm{Res}(g, z_k) \tag{A.35}$$

$$\alpha(\tau) = i \sum_{\Im(z_k) > 0} \mathrm{Res}(g, z_k) \tag{A.36}$$

We insert all the imaginary singularities

$$\alpha(\tau) = i \Big[\mathrm{Res}(g_1, i) + \sum_{k=0}^{\infty} \mathrm{Res}(g_1, 2\pi ik) \Big] \tag{A.37}$$

A.2.1. Residuum at $i\gamma$

mit $0 \neq \gamma \in \mathbb{R} \setminus \mathbb{C}$

The residue of the function $g(z)$ at z_0 is given by:

$$\text{Res}(g, z_0) = \lim_{z \to z_0} (z - z_0) g(z) \tag{A.38}$$

Given $g(z) = \eta \frac{z\gamma}{(z-i\gamma)(z+i\gamma)} \left[\frac{1}{z\beta} + \frac{1}{2}\right] e^{iz\tau}$, we can compute the residue at $z_0 = i\gamma$ as follows:

First, simplify by noting that $(z - i\gamma)$ can be left out:

$$\text{Res}(g, i\gamma) = \lim_{z \to i\gamma} \eta \frac{z\gamma}{(z + i\gamma)} \left[\frac{1}{z\beta} + \frac{1}{2}\right] e^{iz\tau} \tag{A.39}$$

Since $\frac{1}{i\gamma} \neq 0$, there is no additional singularity

Substitute $z = i\gamma$ into the expression:

$$\text{Res}(g, i\gamma) = \eta \frac{(i\gamma)\gamma}{(i\gamma + i\gamma)} \left[\frac{1}{i\gamma\beta} + \frac{1}{2}\right] e^{i(i\gamma)\tau} \tag{A.40}$$

Simplify the expression:

$$\text{Res}(g, i\gamma) = \eta \frac{i\gamma^2}{2i\gamma} \left[\frac{1}{i\gamma\beta} + \frac{1}{2}\right] e^{-\gamma\tau} \tag{A.41}$$

Multiply the $\frac{\gamma^2}{2\gamma}$ inside the parenthesis

$$\text{Res}(g, i\gamma) = \eta \left[\frac{\gamma^2}{2\gamma} \frac{1}{i\gamma\beta} + \frac{\gamma^2}{2\gamma} \frac{1}{2}\right] e^{-\gamma\tau} \tag{A.42}$$

Simplifying

$$\text{Res}(g, i\gamma) = \eta \left[\frac{1}{2i\beta} + \frac{\gamma}{4}\right] e^{-\gamma\tau} \tag{A.43}$$

Bring imaginary unit up

$$\text{Res}(g, i\gamma) = \eta \left[\frac{-i}{2\beta} + \frac{\gamma}{4}\right] e^{-\gamma\tau} \tag{A.44}$$

Separate imaginary and real part:

$$\text{Res}(g, i\gamma) = \left[(-i)\frac{\eta}{2\beta} + \eta\frac{\gamma}{4}\right] e^{-\gamma\tau} \tag{A.45}$$

$$\alpha(\tau) = \frac{1}{\pi} 2\pi i \left[(-i)\frac{\eta}{2\beta} + \eta\frac{\gamma}{4}\right] e^{-\gamma\tau} \tag{A.46}$$

Reduce the factors at the beginning and resolve $i(-i)$ and multiply with i

$$\alpha(\tau) = \left[\frac{\eta}{\beta} + i\eta\frac{\gamma}{2}\right] e^{-\gamma\tau} \tag{A.47}$$

A.3. Derivation for the Ohmic spectral density

$$\alpha(\tau) = \frac{1}{\pi}\int_{-\infty}^{\infty} S(\omega) f_{\text{Bose}}(\omega\beta)\, e^{i\omega\tau} d\omega \tag{A.48}$$

$$\alpha(\tau) = \frac{1}{\pi}\int_{-\infty}^{\infty} \pi\omega e^{-|\frac{\omega}{\Omega}|} \frac{1}{1-e^{-\omega\beta}} e^{i\omega\tau} d\omega \tag{A.49}$$

Positive imaginary singularities appear at $\omega = 2\pi ikT$, $k \in \mathbb{N}^+$ and we define:

$$g(z) = \pi z e^{-|\frac{z}{\Omega}|} \frac{1}{1-e^{-z\beta}} e^{iz\tau} \tag{A.50}$$

$$\alpha(\tau) = \frac{1}{\pi} 2\pi i \left[\sum_{k=0}^{\infty} \text{Res}(g, 2\pi ikT)\right] \tag{A.51}$$

A.3.1. Residuum at $z_k = 2\pi ik$

$$\text{Res}(g_1, 2\pi ikT) = \lim_{z\to 2\pi ikT} (z - 2\pi ikT)\pi z e^{-|\frac{z}{\Omega}|} \frac{1}{1-e^{-z\beta}} e^{iz\tau} \tag{A.52}$$

We split the limes in two, as they are both converging (Fischer & Kaul, p.164) [FK88]

$$= \text{Res}(g_1, 2\pi ikT) = \lim_{z\to 2\pi ikT} (z - 2\pi ikT)\pi z e^{-|\frac{z}{\Omega}|} e^{iz\tau} \lim_{z\to 2\pi ikT} \frac{1}{1-e^{-z\beta}} \tag{A.53}$$

We apply de l'Hospital derivation rule on the second limes, (Fischer & Kaul, p.195) [FK88]

$$= \lim_{z\to 2\pi ikT} \pi z e^{-|\frac{z}{\Omega}|} e^{iz\tau} \lim_{z\to 2\pi ikT} \frac{(z - 2\pi ikT)}{1-e^{-z\beta}} \tag{A.54}$$

We take the derivative:

$$= \lim_{z\to 2\pi ikT} \pi z e^{-|\frac{z}{\Omega}|} \frac{1}{e^{-z\beta}} e^{iz\tau} \tag{A.55}$$

Next, we substitute $z = 2\pi ikT$:

$$= (2\pi^2 ikT) e^{-|\frac{2\pi ik}{\Omega}|} \frac{1}{e^{-(2\pi iT\beta)}} e^{i(2\pi ik)\tau} \tag{A.56}$$

Since $e^{2\pi ikT\beta} = 1$:

$$= (2\pi^2 ikT) e^{-|\frac{2\pi ikT}{\Omega}|} e^{i(2\pi ik)\tau} \tag{A.57}$$

With $i^2 = -1$, we simplify to:

$$= (2\pi^2 ikT)e^{-|\frac{2\pi ikT}{\Omega}|}e^{-(2\pi ikT)\tau} \tag{A.58}$$

Remove the absolutes, with: $|z| = \sqrt{a^2 + b^2}, z = a + ib$

$$= (2\pi^2 ik)e^{-\frac{2\pi kT}{\Omega}}e^{-(2\pi kT)\tau} \tag{A.59}$$

Adding the exponents together

$$= (2\pi^2 ik)e^{-\frac{2\pi kT}{\Omega}-2\pi kT\tau} \tag{A.60}$$

Factor out $-2\pi kT$:

$$= (2\pi^2 ik)e^{-2\pi kT(\frac{1}{\Omega}+\tau)} \tag{A.61}$$

Factoring out constants:

$$= i(2\pi^2 k)e^{-2\pi kT(\frac{1}{\Omega}+\tau)} \tag{A.62}$$

Including the sum of residues and bath scaling factor

$$\alpha(\tau) = \frac{1}{\pi}2\pi i\left[\sum_{k=1}^{\infty} i(2\pi^2 k)e^{-2\pi kT(\frac{1}{\Omega}+\tau)}\right] \tag{A.63}$$

Since $i^2 = -1$:

$$= 2\left[\sum_{k=1}^{\infty} -(2\pi^2 k)e^{-2\pi kT(\frac{1}{\Omega}+\tau)}\right] \tag{A.64}$$

Factor in 2

$$= \left[\sum_{k=1}^{\infty} -4\pi^2 ke^{-2\pi kT(\frac{1}{\Omega}+\tau)}\right] \tag{A.65}$$

Factoring out $-4\pi^2$:

$$\alpha(\tau) = -4\pi^2\sum_{k=1}^{\infty} ke^{-2\pi kT(\frac{1}{\Omega}+\tau)} \tag{A.66}$$

We only use limited approximation terms K

$$\alpha(\tau) = -4\pi^2\sum_{k=1}^{K} ke^{-2\pi kT(\frac{1}{\Omega}+\tau)} \tag{A.67}$$

List of Figures

2.1. Schematics of the system S consisting of the target T, the environment E, and interactions TE_k . . . 2
2.2. Two bath modes as harmonic oscillators with three states at frequency ω_k, each linearly interacting with target T, with coupling strength $L_k\gamma_k$ 3
2.3. Two pendulums at frequencies ω_1 and ω_2 connected to target T by springs representing coupling strengths $L_1\gamma_1$ and $L_2\gamma_2$ . . . 4
2.4. Debye (green curve) and Ohmic (red curve) spectral densities . . . 5
2.5. Laurent expansion for the Bose function with increasing approximation terms n . . . 6
2.6. Structure of the bath correlation function: Spectral density, Fourier transform $e^{i\omega\tau}$, Bose function, and the residue theorem with related sections in the Background . . . 7
2.7. Continuum of bath modes: Each bath mode k represents a frequency ω_k on the spectrum with coupling strength $L_k\gamma_k$ . . . 8
2.8. Schematic representation of the residue theorem: Imaginary singularities are black dots and path integral is represented by the black semi-circle (Fischer & Kaul, p.570) [FK88] . . . 9
2.9. Analogy for the residue theorem . . . 10

4.1. Pyramid structure of the bath correlation function with respective sections 13
4.2. Real and imaginary part: Comparing integral limits . . . 14
4.3. Real and imaginary part: Distance to singularity . . . 14
4.4. Real and imaginary part: Compare numerical reference with residue decomposition . . . 15
4.5. Real and imaginary part: Error rates of the residue decomposition . . . 16
4.6. Influences of terms: Real and Imaginary Part . . . 16
4.7. Column diagram of the four data series . . . 17
4.8. Real and imaginary part: Compare numerical reference with Laurent expansions . . . 18
4.9. Real and imaginary part: Compare numerical reference with residue decomposition . . . 19
4.10. Real and imaginary part: Error rates of the residue decomposition . . . 19

4.11. Temperature Comparison for Debye spectral density: Real and Imaginary Part 20
4.12. Temperature Comparison for Debye spectral density: Real and Imaginary Part 21
4.13. Temperature Comparison for Ohmic spectral density: Real and Imaginary Part 22

Bibliography

[Bla24] B. Blaschko. *Decomposition: Methods to Approximate the Exponential Sum Bath Correlation Function*. `https://github.com/beneblaschk/bath_correlation_decomposition`. 2024 (cit. on p. 1).

[BPW96] W. P. de Boeij, M. S. Pshenichnikov, and D. A. Wiersma. "System- Bath Correlation Function Probed by Conventional and Time-Gated Stimulated Photon Echo." In: *The Journal of Physical Chemistry* 100.29 (1996), pp. 11806–11823 (cit. on p. 12).

[Bre+84] J. Bretón, A. Hardisson, F. Mauricio, and S. Velasco. "Relaxation of quantum systems weakly coupled to a bath. I. Total-time-ordering-cumulant and partial-time-ordering-cumulant non-Markovian theories." In: *Physical Review A* 30.1 (1984), p. 542 (cit. on pp. 1, 12).

[Cui+20] J. Cui, Z. Gong, R.-X. Xu, X. Zheng, and Y. Yan. "Hierarchical equations of motion method based on Fano spectrum decomposition for low temperature environments." In: *Journal of Chemical Physics* (2020) (cit. on p. 11).

[Dim13] A. Dimca. *Topics on real and complex singularities: an introduction*. Springer-Verlag, 2013 (cit. on p. 5).

[DPW12] N. S. Dattani, F. A. Pollock, and D. M. Wilkins. "Analytic influence functionals for numerical Feynman integrals in most open quantum systems." In: *arXiv preprint arXiv:1203.4551* (Mar. 2012). Submitted on 20 Mar 2012, 11 pages, 1 figure, 4 footnotes, 35 references. DOI: `10.48550/arXiv.1203.4551`. arXiv: `1203.4551 [quant-ph]` (cit. on p. 11).

[Fay22] T. P. Fay. "A simple improved low temperature correction for the hierarchical equations of motion." In: *The Journal of Chemical Physics* 157.5 (2022) (cit. on p. 11).

[FK88] H. Fischer and H. Kaul. *Mathematik für Physiker Band 1: Grundkurs*. 7th. Reprinted 2011. University of Tübingen: Springer, 1988 (cit. on pp. 5, 9, 26, 27, 31).

[GM06] J. B. Gilmore and R. H. McKenzie. "Criteria for quantum coherent transfer of excitations between chromophores in a polar solvent." In: *Chemical Physics Letters* 421.1–3 (Apr. 2006), pp. 266–271. DOI: 10.1016/j.cplett.2006.01.067. URL: https://doi.org/10.1016/j.cplett.2006.01.067 (cit. on pp. 1, 2, 12).

[GOA94] A. Garg, J. N. Onuchic, and V. Ambegaokar. "Effect of friction on electron transfer in biomolecules." In: *Chemical Physics* 182.2–3 (May 1994), pp. 91–117. DOI: 10.1016/0301-0104(94)00016-6. URL: https://doi.org/10.1016/0301-0104(94)00016-6 (cit. on pp. 2, 3).

[GPW99] M. Grifoni, E. Paladino, and U. Weiss. "Dissipation, decoherence and preparation effects in the spin-boson system." In: *The European Physical Journal B-Condensed Matter and Complex Systems* 10 (1999), pp. 719–729 (cit. on p. 2).

[HXY10] J. Hu, R.-X. Xu, and Y. Yan. "Communication: Padé spectrum decomposition of Fermi function and Bose function." In: *Journal of Chemical Physics* (2010) (cit. on pp. 6, 7, 18, 24).

[KBT22] Y. Ke, R. Borrelli, and M. Thoss. "Hierarchical equations of motion approach to hybrid fermionic and bosonic environments: Matrix product state formulation in twin space." In: *The Journal of Chemical Physics* 156.19 (2022), p. 194102. DOI: 10.1063/5.0088947 (cit. on p. 11).

[Le +24] B. Le Dé, A. Jaouadi, E. Mangaud, A. W. Chin, and M. Desouter-Lecomte. "Managing temperature in open quantum systems strongly coupled with structured environments." In: *The Journal of Chemical Physics* 160.24 (2024) (cit. on pp. 5, 24).

[Leg+87] A. J. Leggett, S. Chakravarty, A. T. Dorsey, M. P. A. Fisher, A. Garg, and W. Zwerger. "Dynamics of the dissipative two-state system." In: *Reviews of Modern Physics* 59.1 (Jan. 1987). Erratum: Rev. Mod. Phys. 67, 725 (1995), pp. 1–85. DOI: 10.1103/RevModPhys.59.1. URL: https://doi.org/10.1103/RevModPhys.59.1 (cit. on p. 2).

[MT99] C. Meier and D. J. Tannor. "Non-Markovian evolution of the density operator in the presence of strong laser fields." In: *The Journal of Chemical Physics* 111.8 (1999), pp. 3365–3376. DOI: 10.1063/1.479669. URL: http://dx.doi.org/10.1063/1.479669 (cit. on p. 23).

[RE14] G. Ritschel and A. Eisfeld. "Analytic Representations of Bath Correlation Functions for Ohmic and Superohmic Spectral Densities Using Simple Poles." In: *Journal of Chemical Physics* (2014) (cit. on pp. 8, 11, 12).

[Rit+11] G. Ritschel, J. Roden, W. T. Strunz, and A. Eisfeld. "An efficient method to calculate excitation energy transfer in light harvesting systems. Application to the FMO complex." In: *New Journal of Physics* 13 (2011), p. 113034. DOI: 10.1088/1367-2630/13/11/113034. arXiv: 1106.5259 [quant-ph] (cit. on p. 11).

[Sap23] B. Sappler. *Benchmarking a Tensor Network Algorithm for the HOPS-Method to Simulate Open Non-Markovian Quantum Systems*. 2023 (cit. on pp. 3, 5, 8, 12, 15, 18, 20, 23, 24, 29).

[SCE15] D. W. Schönleber, A. Croy, and A. Eisfeld. "Pseudomodes and the corresponding transformation of the temperature-dependent bath correlation function." In: *Physical Review A* 91 (May 2015). Received 7 April 2015, p. 052108. DOI: 10.1103/PhysRevA.91.052108 (cit. on pp. 1–3, 7, 12).

[Sci24] SciPy Documentation Team. *SciPy Integrate and ODE Solvers Tutorial*. Accessed: 2024-09-03. 2024. URL: https://docs.scipy.org/doc/scipy/tutorial/integrate.html (cit. on pp. 13, 23).

[SES14] D. Süß, A. Eisfeld, and W. T. Strunz. "Hierarchy of stochastic pure states for open quantum system dynamics." In: *Physical Review Letters* (2014) (cit. on pp. 1, 8, 12, 15, 24).

[Shi+09] Q. Shi, L. Chen, G. Nan, R. Xu, and Y. Yan. "Electron transfer dynamics: Zusman equation versus exact theory." In: *The Journal of chemical physics* 130.16 (2009) (cit. on p. 4).

[SS11] J. Strümpfer and K. Schulten. "The effect of correlated bath fluctuations on exciton transfer." In: *Journal of Chemical Physics* (2011) (cit. on pp. 1, 12).

[SV10] A. Smirne and B. Vacchini. "Nakajima-Zwanzig versus time-convolutionless master equation for the non-Markovian dynamics of a two-level system." In: *Physical Review A* 82 (Aug. 2010). Received 10 May 2010, p. 022110. DOI: 10.1103/PhysRevA.82.022110 (cit. on p. 11).

[Tan90] Y. Tanimura. "Nonperturbative expansion method for a quantum system coupled to a harmonic-oscillator bath." In: *Physical Review A* 41.12 (1990), p. 6676 (cit. on p. 11).

[Wan+99] H. Wang, X. Song, D. Chandler, and W. H. Miller. "Semiclassical study of electronically nonadiabatic dynamics in the condensed-phase: Spin-boson problem with Debye spectral density." In: *The Journal of Chemical Physics* 110.10 (Mar. 1999), pp. 4828–4840. DOI: 10.1063/1.478388 (cit. on pp. 4, 5, 24).

[Wei12] U. Weiss. *Quantum dissipative systems*. World Scientific, 2012 (cit. on p. 12).

[WKV04] F. Wilhelm, S. Kleff, and J. Von Delft. "The spin-boson model with a structured environment: a comparison of approaches." In: *Chemical physics* 296.2-3 (2004), pp. 345–353 (cit. on pp. 1, 4).

[XS94] D. Xu and K. Schulten. "Coupling of protein motion to electron transfer in a photosynthetic reaction center: investigating the low temperature behavior in the framework of the spin–boson model." In: *Chemical Physics* 182.2–3 (May 1994), pp. 91–117. DOI: 10.1016/0301-0104(94)00016-6. URL: https://doi.org/10.1016/0301-0104(94)00016-6 (cit. on pp. 1, 12).

[XY07] R.-X. Xu and Y. Yan. "Dynamics of quantum dissipation systems interacting with bosonic canonical bath: Hierarchical equations of motion approach." In: *Physical Review E* 75 (Mar. 2007). Received 24 October 2006, p. 031107. DOI: 10.1103/PhysRevE.75.031107 (cit. on p. 11).

[Zha+21] N.-N. Zhang, M.-J. Tao, W.-T. He, X.-Y. Chen, X.-Y. Kong, F.-G. Deng, N. Lambert, and Q. Ai. "Efficient quantum simulation of open quantum dynamics at various Hamiltonians and spectral densities." In: *Scientific Reports* 16 (Mar. 2021). Research Article, Published 30 March 2021, p. 51501. DOI: 10.1038/srep51501 (cit. on p. 4).